Enhancing Inner-Rotor Radial Flux PMSG Design through Air-Gap Flux Validation and Leakage Inductance Modeling

Hari Prasetijo
Department of Electrical Engineering, Universitas Jenderal Soedirman, Purwokerto, Indonesia | Doctoral Program in Ilmu Teknik, Universitas Negeri Yogyakarta, Yogyakarta, Indonesia
hari.prasetijo@unsoed.ac.id

Mohammad Khairudin
Department of Electrical Engineering, Universitas Negeri Yogyakarta, Yogyakarta, Indonesia
moh_khairudin@uny.ac.id (corresponding author)

Ketut Wirtayasa
Research Center for Energy Conversion and Conservation, National Research and Innovation Agency, Bandung, Indonesia
ketu003@brin.go.id

Daru Tri Nugroho
Department of Electrical Engineering, Universitas Jenderal Soedirman, Purwokerto, Indonesia
daru.nugroho@unsoed.ac.id

Yogi Ramadhani
Department of Electrical Engineering, Universitas Jenderal Soedirman, Purwokerto, Indonesia
yogi.ramadhani@unsoed.ac.id

Received: 24 June 2025 | Revised: 1 August 2025 | Accepted: 14 August 2025

 DOI: https://doi.org/10.48084/etasr.12899

ABSTRACT

This study presents a comprehensive design and performance validation of a three-phase, 900-watt Inner-Rotor Radial Flux Surface-Mounted Permanent Magnet Synchronous Generator (IR-RF-SPMSG). The proposed generator, featuring 10 poles and 30 slots with a 0.9 pole arc ratio, is designed analytically and simulated using 3D finite element modeling. The key contributions include the validation of the air-gap flux density using leakage and reluctance correction factors, the detailed modeling of the leakage inductance components, and an accurate three-phase winding configuration. The comparison between the analytical and simulation results yields errors below 1% for the air-gap flux density (B_g), back-EMF (E_{ph}), phase current (I_{ph}), terminal voltage (V_{ph}), and three-phase output power (S_{out}). The methodology significantly improves the terminal voltage prediction under load and ensures waveform integrity, offering a reliable design reference for low-speed renewable energy systems.

Keywords-radial flux generator; flux validation; leakage inductance; FEM simulation; low-speed design; renewable energy

I. INTRODUCTION

The rising demand for small-scale renewable energy systems has led to an increasing need for low-speed permanent magnet generators optimized for direct-drive operation. One effective approach to achieving low rotational speeds is by increasing the number of poles in the generator, thereby reducing or eliminating the need for mechanical gearboxes and improving the overall system efficiency [1, 2]. The IR-RF-SPMSG is particularly attractive because it eliminates the excitation windings and slip rings, resulting in improved mechanical reliability, reduced maintenance, and simplified construction [3-5]. Its radial flux configuration not only enhances the manufacturability and structural strength, but also

supports higher torque density and efficient magnetic utilization, which are critical in compact, low-speed renewable energy applications [6, 7]. Moreover, surface-mounted permanent magnets are well-suited for low-speed operation due to their minimal exposure to centrifugal forces, straightforward assembly process, and ability to maintain stable air-gap flux density, making them ideal for robust and cost-effective generator designs in distributed energy systems [8].

The air-gap flux density (B_g) is significantly influenced by the magnet's shape, placement, and size, as these parameters directly determine the distribution and magnitude of the magnetic field in the active region of the machine [9-11]. High-performance NdFeB magnets are commonly employed in such designs due to their superior energy product, which supports compact geometries, high torque density, and enhanced overall efficiency [12-14]. Additionally, magnetically soft steel is extensively utilized in stator and rotor cores for its high permeability and low hysteresis loss, ensuring efficient magnetic coupling and reduced core losses, which are essential for stable flux linkage and precise back-EMF generation in low-speed permanent magnet generators [15, 16].

Several studies have proposed IR-RF-SPMSG designs with varying objectives, including efficiency improvement, size reduction, and performance optimization for renewable energy applications. However, many of these works overlook the critical aspects that directly influence the analytical accuracy and practical reliability, such as rigorous flux density validation to ensure correct electromagnetic field representation, comprehensive leakage inductance modeling that accounts for air-gap, slot, and end-winding effects, and precise winding configuration necessary to preserve phase balance and waveform integrity [17–24]. Authors in [25] explained the winding configuration but did not validate the flux density or calculate the leakage inductance. Most studies rely on simplified 2D simulations, low-coercivity magnets, or do not evaluate the performance under load conditions.

Research further emphasizes that precise modeling is essential. In a grid-tied PMSG study, authors in [26] linked the reactive power support to the grid-compliant design, whereas swarm intelligence optimization [27] improved dynamic response and power quality, and SSA with fuzzy logic [28] enhanced LVRT and flux regulation—collectively reinforcing the need for a rigorous flux validation and inductance modeling to ensure a reliable generator performance.

This study aims to enhance the design accuracy by validating B_g and performing detailed modeling of the leakage inductance—covering the air-gap, slot, tooth tip, and end winding components. In addition, the accurate modeling of the three-phase winding arrangement is emphasized to ensure the waveform integrity and prevent phase cancellation. A 900 W, 10-pole, 30-slot IR-RF-SPMSG operating at 600 rpm is designed analytically and validated through 3D finite element analysis. This integrated method addresses the gaps in prior work and enables more accurate prediction of the back-EMF and terminal voltage under load conditions.

II. METHODOLOGY

This study employs an integrated approach combining analytical calculations and 3D finite element simulations to improve the design accuracy of an IR-RF-SPMSG. The input parameters of the generator are rated at 900 W. It features 10 poles, 30 stator slots, and operates at 600 rpm. NdFeB 35H magnets are used with an air gap of 1.5 mm. Magnetic and structural core materials are selected from JFE Steel 50JN470, with B-H characteristics sourced from the Ansys Maxwell material library.

Based on the input parameters, the design process begins with calculating dimensional parameters, such as the rotor diameter, stator slot geometry, and magnet dimensions based on electrical and magnetic loading. These parameters are then used to construct a 3D model in Ansys Maxwell. The magnetic parameters focus on validating the air-gap flux density (B_g), using analytical equations corrected by Carter's coefficient and reluctance factor, followed by magnetic flux (ϕ) calculation.

Based on the dimensional parameters, the electrical parameter calculation includes back-EMF (E_{ph}), phase current (I_{ph}), resistance (R_{ph}), and inductance (L_{ph}). Special emphasis is placed on leakage inductance modeling, which comprises air-gap, slot, tooth-tip, and end-winding components. These values are calculated analytically and manually incorporated into the simulation model to refine the voltage drop (ΔV_{ph}), terminal voltage (V_{ph}), and voltage regulation (V_R).

Winding configuration is precisely modeled through a 30-slot double-layer star-of-slot arrangement. The correct coil phasing ensures that the back-EMF waveforms are accurate and in-phase. The modeling ensures alignment between the simulated and analytical results.

Performance metrics—including B_g, E_{ph}, I_{ph}, V_{ph}, and S_{out}—are validated through simulation. Parameters are evaluated on a per-phase basis. The comprehensive method ensures high fidelity between the analytical design and finite element analysis results by addressing often-overlooked factors, such as inductive effects and winding layout precision.

III. RESULT

The analytical design produced key dimensional, magnetic, and electrical parameters for a 900 W, 10-pole, 30-slot IR-RF-SPMSG operating at 600 rpm and 220 V. Dimensional parameters, such as the stator inner diameter, rotor outer diameter, slot geometry, and magnet dimensions were computed using standard electromagnetic machine design equations. The key calculated dimensions included a stator inner diameter of 155 mm and a stack length of 57.7 mm, with a pole arc ratio of 0.9 to minimize the flux leakage between adjacent poles.

The magnetic parameter validation focused on the air-gap flux density (B_g). The analytically calculated B_g using (1) was 0.973 tesla (T) assuming no leakage (k_{ml} = 1):

$$B_g = \frac{C_\phi}{1+\frac{\mu_r + k_C + k_{ml}}{PC}} x B_r \quad (1)$$

The simulation via Ansys Maxwell returned a value of 0.831 T, leading to a calculated leakage factor (K_l) of 0.857, indicating that 85.7% of the generated flux reaches the air gap. After applying reluctance factor correction, the validated B_g using (2) was 0.836 T, yielding a percentage error of 0.48% against simulation. The corresponding magnetic flux was 0.002 Wb, which was then used to calculate the electric parameters:

$$B_g = \frac{K_l C_\phi}{1+K_r \frac{\mu_r}{P_c}} x B_r \quad (2)$$

From the geometry generator, carter's coefficient (k_c) was 1.11 and permeance coefficient (P_c) was 8. With a pole arc ratio of 0.9, the flux concentrated factor C_ϕ was 0.95. The reluctance factor (K_r) was 1.1 as a moderate value. The residual magnetic flux density (B_r) and relative recoil permeability (μ_r) of NdFeB 35H were 1.18 T and 1.07, respectively:

$$E_{ph} = 4.44 x f x k_w x \phi = 235.8 \text{ volt} \quad (3)$$

$$I_{ph} = \frac{P}{3.m.E_{ph}.cos\theta} = 1.6043 \text{ A} \quad (4)$$

$$L_m = \alpha_i \frac{m \tau_p}{\pi p^2 l_g} \mu_0 L_i (k_w N_s)^2 \quad (5)$$

$$L_\delta = \frac{\mu_0}{\pi} \frac{m}{l_g} D L_i \left(\frac{N}{p}\right)^2 k_w^2 = 0.000763 \text{ H} \quad (6)$$

$$L_u = \frac{4m}{Q} \mu_0 L_i N^2 \lambda_u = 0.000026 \text{ H} \quad (7)$$

$$L_d = \frac{4m}{Q} \mu_0 l' N^2 \lambda_d = 0.001089 \text{ H} \quad (8)$$

$$L_w = \frac{2}{Qp} N^2 \mu_0 l_w \lambda_w = 0.000001 \text{ H} \quad (9)$$

$$L_\sigma = L_\delta + L_u + L_d + L_w = 0.001883 \text{ H} \quad (10)$$

$$L_{total} = 10(L_m + L_\sigma) = 0.026466 \, H \quad (11)$$

$$X_L = 2\pi f L_{total} = 8.3 \text{ ohm} \quad (12)$$

$$r_{ph} = \frac{\rho . l_w}{A_w} = 1.6 \text{ ohm} \quad (13)$$

$$\Delta V_{ph} = I_{ph} x (r_{ph} + jX_{ph}) = 13.6 \text{ volt} \quad (14)$$

$$V_{ph} = E_{ph} - I_{ph} x (r_{ph} + jX_{ph}) = 222.3 \text{ volt} \quad (15)$$

Calculations in the analytical design were conducted on per-phase basis parameters and the results are shown in (3-15). The total leakage inductance (L_{leak}) was derived by summing the leakage inductance at air-gap (L_δ) = 0.000764 Henry (H), slot (L_u) = 0.000026 H, tooth tip (L_d) = 0.001089 H, and end-winding (L_w) = 0.000001 H. Total leakage inductance was: L_σ = 0.001883 H. Including main inductance was: L_m = 0.00764 H, and the total inductance was: L_{total} = 0.026466 H.

The winding configuration was modeled using a double-layer lap winding with a coil pitch of 3. The 30-slot stator was divided into symmetrical groups to form three balanced phases. Using a star-of-slot representation in Figure 1, phasors were mapped to determine the correct slot pairings for each phase, ensuring in-phase back-EMF and avoiding cancellation.

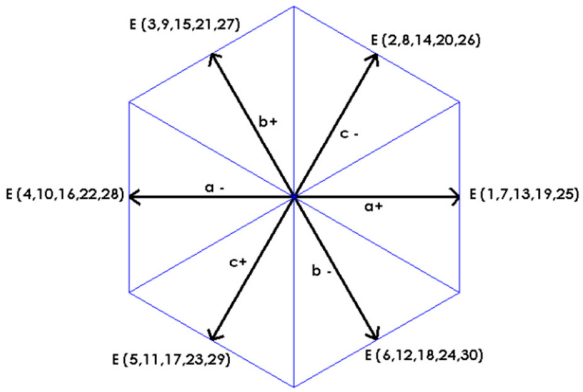

Fig. 1. Star-of-slot 3 phase winding (30 slot double layer).

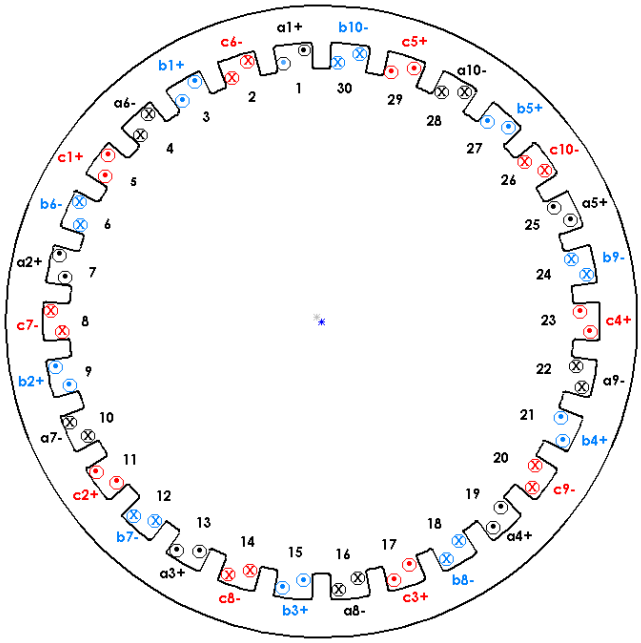

Fig. 2. Stator winding 3 phase 30 slot, double winding.

Figure 2 shows the stator winding based on the star-of-slot. Phase A, for instance, used slots 1, 7, 13, 19, and 25 for positive coil sides and 4, 10, 16, 22, and 28 for negative ones. The accurate placement of these coils was critical to preserving the waveform integrity in the simulation. The analytical design results were validated through 3D simulation. The analytical value of the air-gap flux density (B_g), calculated using (2), was 0.836 T, while the 3D simulation result was 0.832 T, as depicted in Figure 3. Similarly, the analytical back-EMF (E_{ph}) value, calculated using (3), was 235.8 V. The simulated back-EMF waveforms for phases A, B, and C, portrayed in Figure 4, were 234.9 V, 234.7 V, and 234.4 V, respectively. The minimal deviation from the 235.8 V reference confirms the high accuracy of the analytical back-EMF prediction under specified design conditions. This result clearly demonstrates that the analytical design was reliably validated by detailed 3D simulation.

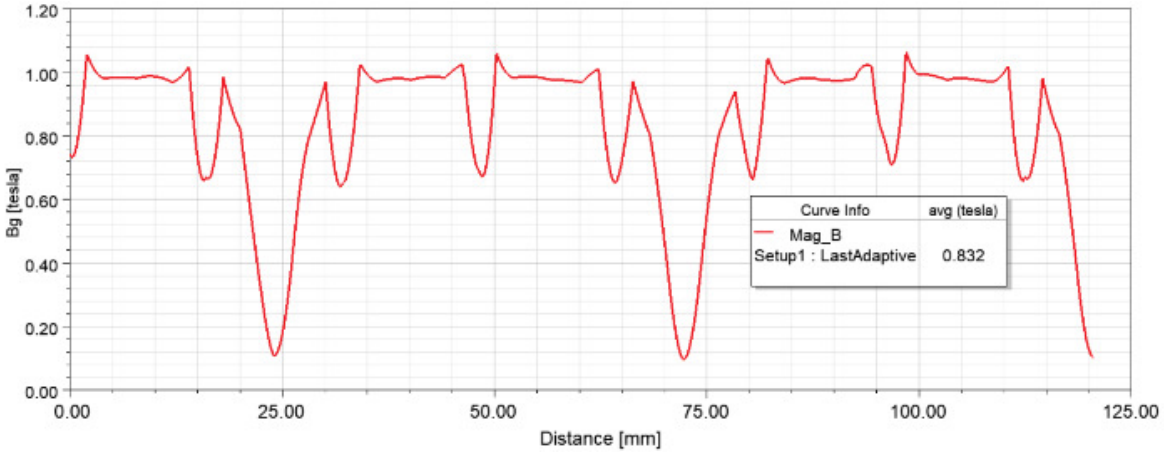

Fig. 3. Simulation result of air-gap flux density (B_g).

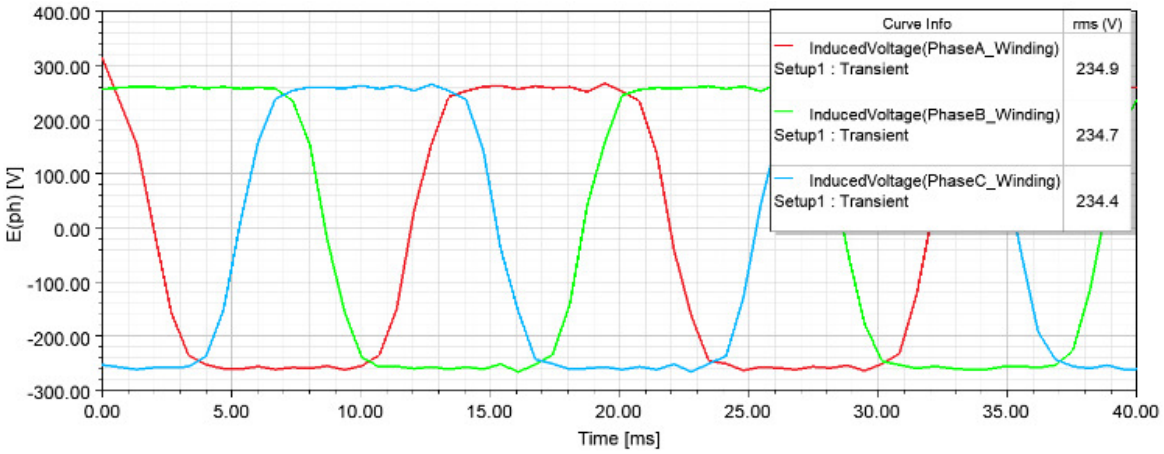

Fig. 4. Back-EMF waveforms.

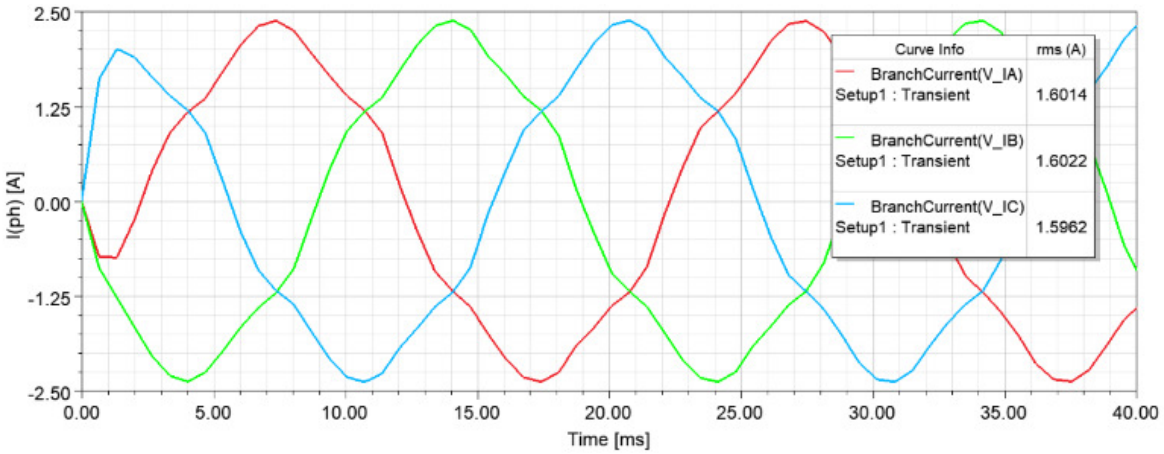

Fig. 5. Phase load current (I_{ph}).

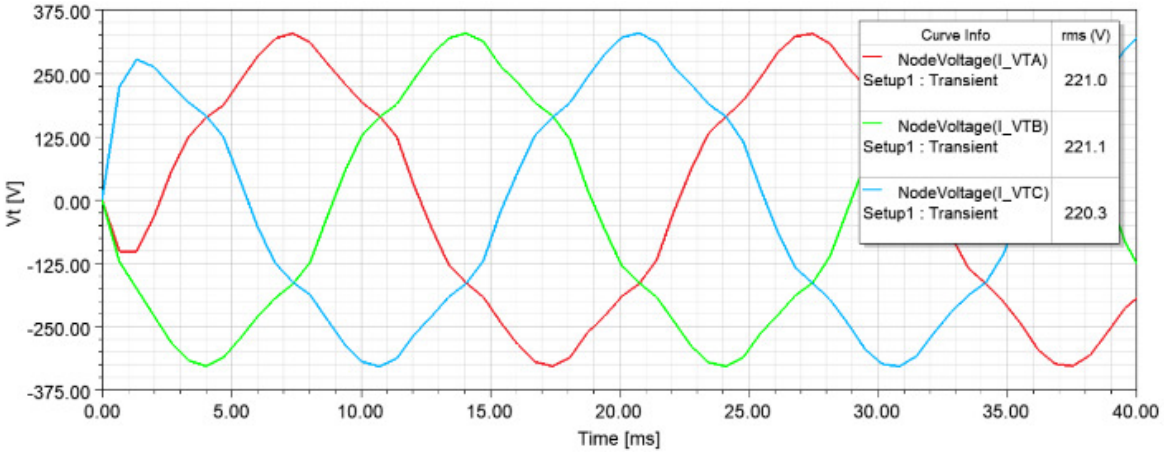

Fig. 6. Terminal voltage (V_{ph}) waveforms.

The simulated phase currents (I_{ph}), as presented in Figure 5, were 1.6014 A for phase A, 1.6022 A for phase B, and 1.5962 A for phase C. The analytical phase current, calculated using (4) was 1.6043 A. Likewise, the simulated terminal voltages (V_{ph}), as displayed in Figure 6, were 221.0 V for phase A, 221.1 V for phase B, and 220.3 V for phase C. The analytical terminal voltage, calculated using (15), was 222.3 V. Finally, the total three-phase output power obtained from the simulation was 1060.3 VA, which closely matched the analytically predicted value of 1058.8 VA.

IV. DISCUSSION

The proposed IR-RF-SPMSG analytical design was evaluated by comparing key performance parameters—including air-gap flux density (B_g), back-EMF (E_{ph}), phase current (I_{ph}), terminal voltage (V_{ph}), and three-phase output power (S_{out})—between the analytically derived values and high-fidelity 3D finite element simulations conducted in ANSYS Maxwell. The results exhibited a high degree of agreement, confirming the exceptional accuracy of the analytical design across multiple critical performance metrics and operating conditions. This strong correlation further demonstrates its robustness and reliability as a rigorously validated methodology for advanced permanent magnet generator development, precise electromagnetic performance prediction, enhanced design optimization, and practical renewable energy system integration worldwide.

The simulation model includes a rotor with ten surface-mounted permanent magnets in alternating polarities (five north, five south), a 30-slot stator, and a three-phase winding with ten coils per phase. A double-layer lap winding with a coil pitch of three was applied. Accurate modeling of the winding configuration—including coil phasing and slot pairing—was critical to the waveform generation and to avoiding phase cancellation. The average air-gap flux density (B_g) from the analytical design was 0.836 T, closely matching the simulated 0.832 T, with a 0.48% deviation. This small discrepancy shows that the analytical design—accounting for reluctance and flux leakage—is well represented in the simulation. These results confirm that the flux density estimation can be reliably achieved through a combined analytical and simulation-based approach.

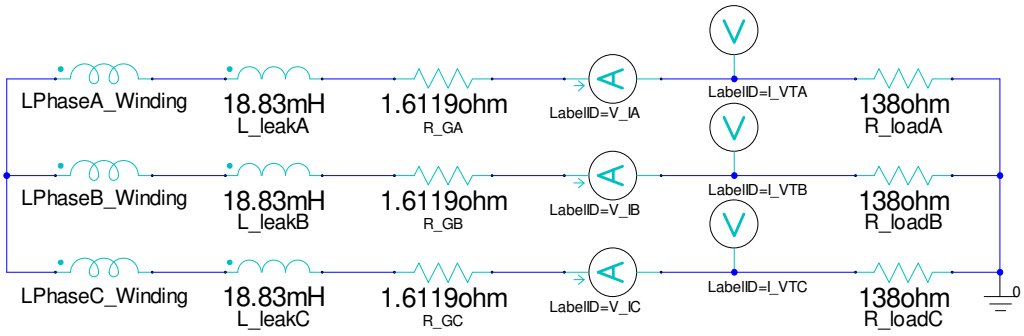

Fig. 7. Equivalent circuit model of the generator.

The back-EMF (E_{ph}) results showed strong agreement between the analytical predictions and simulations, with minor deviations (0.38%–0.60%) from the calculated 235.8 V. These small errors are mainly due to the improved reluctance modeling, which accounts for stator teeth saturation and air-gap fringing. The findings confirm that an accurate B_g estimation is essential for a reliable back-EMF prediction.

The phase current results (I_{ph}), obtained under a 138 Ω resistive load, showed near-identical values between the

analytical design calculation and simulation. The respective errors were 0.181% for phase A, 0.131% for phase B, and 0.505% for phase C. This close agreement underscores the accuracy of the inductance modeling, particularly the explicit incorporation of leakage inductance into the simulation circuit.

The analytical terminal voltage (V_{ph}) of 222.3 V deviated by only 0.59%–0.91% from the simulated values of 221.0 V, 221.1 V, and 220.3 V for phases A, B, and C, demonstrating exceptional accuracy across the phases. This agreement results from the precise and comprehensive leakage inductance modeling, a critical factor in accurately predicting the voltage drop under realistic load conditions, as illustrated in Figure 7. Earlier studies frequently omitted this essential aspect, leading to overestimated analytical predictions and reduced reliability in permanent magnet generator design validation.

The analytical three-phase output power (S_{out}) was 1058.8 VA, closely matching the simulated 1060.3 VA (0.14% deviation). The power was computed from the sum of the phase currents and terminal voltages across phases A, B, and C. This agreement confirms the accuracy of both the design and simulation. The manual inductance estimates and precise coil modeling produced a simulation that reflects real conditions. The key analytical and simulated parameters are summarized in Table I.

Compared to similar studies, this work demonstrates improved accuracy and broader validation. The reported deviations include flux density (B_g) errors of 4.35% [20], 1.15% [21], and 0.29% [24]; back-EMF (E_{ph}) errors of 3.00% [20] and 6.94% [22]; phase current error (I_{ph}) of 2.06% [24]; and output power (S_{out}) error of 4.89% [24]. Other studies [17–19, 23, 25] used analytical and finite element analysis methods without reporting their accuracy. This study achieves sub-1% errors across B_g, E_{ph}, I_{ph}, V_{ph}, and S_{out}—offering a more rigorous and comprehensive validation.

The results confirm that neglecting the flux density validation, leakage inductance, or improper coil placement can cause significant simulation errors. This study shows that with thorough validation and accurate magnetic and electrical modeling, the finite element simulations replicate the real generator behavior.

TABLE I. COMPARISON OF ANALYTICAL DESIGN AND SIMULATION RESULTS

Parameter	Calculation	Simulation	Unit	Error (%)
B_g	0.836	0.832	T	0.48
E_{ph} A	235.8	234.9	V	0.38
E_{ph} B	235.8	234.7	V	0.47
E_{ph} C	235.8	234.4	V	0.60
V_{ph} A	222.3	221.0	V	0.59
V_{ph} B	222.3	221.1	V	0.54
V_{ph} C	222.3	220.3	V	0.91
I_{ph} A	1.6043	1.6014	A	0.181
I_{ph} B	1.6043	1.6022	A	0.131
I_{ph} C	1.6043	1.5962	A	0.505
S_{out}	1058.8	1060.3	VA	0.14

V. CONCLUSION

This study addressed the need for the accurate design of Inner-Rotor Radial Flux Surface-Mounted Permanent Magnet Synchronous Generator (IR-RF-SPMSG) for low-speed renewable energy applications by combining analytical modeling and 3D finite element method validation. The proposed methodology incorporated flux density validation using leakage and reluctance corrections, comprehensive leakage inductance modeling, and precise winding configuration. The key results demonstrated sub-1% errors in the air-gap flux density, back-EMF, phase current, terminal voltage, and output power, confirming the high analytical fidelity. Compared to prior works that reported higher deviations or lacked inductance and flux validation, this study provides a more rigorous framework with improved predictive accuracy. Its novelty lies in integrating detailed inductance modeling and flux validation, offering a reliable reference for accurate PMSG design and performance prediction in practical renewable energy systems.

Future studies should integrate dynamic and thermal analyses to evaluate the generator performance under varying load and environmental conditions. Prototyping and experimental validation are crucial to confirm the flux accuracy and voltage prediction in real operation. Moreover, adopting advanced control strategies and exploring material or design scalability will further enhance the efficiency and broaden the applicability in renewable energy systems.

ACKNOWLEDGMENT

The authors express their gratitude to LPPM UNSOED for funding this research through contract 10.33/UN23.34/ PT.01/VI/2025.

REFERENCES

[1] F. Meier, *Permanent-magnet Synchronous Machines with Non-overlapping Concentrated Windings for Low-Speed Direct-drive Applications*, Stockholm: School of Electrical Engineering, Electrical Machines and Power Electronics, Kungliga Tekniska högskolan, 2008.

[2] K. Wirtayasa and C.-Y. Hsiao, "Performances Comparison of Axial-flux Permanent-magnet Generators for Small-scale Vertical-axis Wind Turbine," *Alexandria Engineering Journal*, vol. 61, no. 2, pp. 1201–1215, Feb. 2022, https://doi.org/10.1016/j.aej.2021.06.074.

[3] S. A. Hussien, M. A. Deab, and F. Alrowais, "Maximization of the Power Delivered from Permanent Magnet Synchronous Generator Wind Energy Conversion System to the Grid Based on Using Moth Flame Optimization," *Indonesian Journal of Electrical Engineering and Computer Science*, vol. 27, no. 3, Sept. 2022, Art. no. 1347, https://doi.org/10.11591/ijeecs.v27.i3.pp1347-1357.

[4] F. Demmelmayr, M. Troyer, and M. Schroedl, "Advantages Of PM-machines Compared to Induction Machines in Terms of Efficiency and Sensorless Control in Traction Applications," in *IECON 2011-37th Annual Conference of the IEEE Industrial Electronics Society*, Melbourne, Australia, Nov. 2011, pp. 2762–2768, https://doi.org/10.1109/IECON.2011.6119749.

[5] H. Polinder, F. F. A. Van Der Pijl, G.-J. De Vilder, and P. J. Tavner, "Comparison of Direct-drive and Geared Generator Concepts for Wind Turbines," *IEEE Transactions on Energy Conversion*, vol. 21, no. 3, pp. 725–733, Sept. 2006, https://doi.org/10.1109/TEC.2006.875476.

[6] M. Mueller and A. Zavvos, "Electrical Generators for Direct Drive Systems: A Technology Overview," in *Electrical Drives for Direct Drive Renewable Energy Systems*, Elsevier, 2013, pp. 3–29.

[7] Y. Wei, Z. Cheng, J. Si, F. Jin, C. Gao, and C. Gan, "Analysis of a Direct-drive Permanent Magnet Synchronous Generator with Novel Toroidal Winding," *IET Renewable Power Generation*, vol. 15, no. 10, pp. 2237–2245, July 2021, https://doi.org/10.1049/rpg2.12158.

[8] A. Bensalah, G. Barakat, and Y. Amara, "Electrical Generators for Large Wind Turbine: Trends and Challenges," *Energies*, vol. 15, no. 18, Sept. 2022, Art. no. 6700, https://doi.org/10.3390/en15186700.

[9] A. J. Sorgdrager and A. J. Grobler, "Influence of Magnet Size and Rotor Topology on the Air-gap Flux Density of a Radial Flux PMSM," in *2013 IEEE International Conference on Industrial Technology*, Cape Town, South Africa, Feb. 2013, pp. 337–343, https://doi.org/10.1109/ICIT.2013.6505695.

[10] B. Singh and S. K. Dwivedi, "A State of Art on Different Configurations of Permanent Magnet Brushless Machines," *Journal of the Institution of Engineers (India): Electrical Engineering Division*, vol. 87, pp. 63–73, June 2006.

[11] C. Soemphol, A. Nuan-on, and P. Parametpisit, "A Prototype Of 3D-printed Permanent Magnet Generator for Low Power Applications," *Indonesian Journal of Electrical Engineering and Computer Science*, vol. 25, no. 1, Jan. 2022, Art. no. 98, https://doi.org/10.11591/ijeecs.v25.i1.pp98-104.

[12] D. Egorov *et al.*, "Hysteresis Loss in NdFeB Permanent Magnets in a Permanent Magnet Synchronous Machine," *IEEE Transactions on Industrial Electronics*, vol. 69, no. 1, pp. 121–129, Jan. 2022, https://doi.org/10.1109/TIE.2021.3050358.

[13] B. Lv, L. Shi, L. Li, K. Liu, and J. Jing, "Performance Analysis of Asymmetrical Less-rare-earth Permanent Magnet Motor for Electric Vehicle," *IET Electrical Systems in Transportation*, vol. 12, no. 1, pp. 36–48, Mar. 2022, https://doi.org/10.1049/els2.12036.

[14] T. Z. Htet, Z. Zhao, and K. Li, "PM Material Analysis of Permanent Magnet Synchronous Generator in Wind Turbines," in *2017 2nd International Conference on System Reliability and Safety*, Milan, Italy, Dec. 2017, pp. 332–336, https://doi.org/10.1109/ICSRS.2017.8272844.

[15] X. Ding, H. Guo, M. Du, B. Li, G. Liu, and L. Zhao, "Effect of Saturation on Iron Loss in PMSM," in *2014 17th International Conference on Electrical Machines and Systems*, Hangzhou, China, Oct. 2014, pp. 3356–3360, https://doi.org/10.1109/ICEMS.2014.7014071.

[16] E. Krol and R. Rossa, "Modern Magnetic Materials in Permanent Magnet Synchronous Motors," in *The XIX International Conference on Electrical Machines - 2010*, Rome, Italy, Sept. 2010, pp. 1–3, https://doi.org/10.1109/ICELMACH.2010.5607962.

[17] H. Prasetijo, W. Winasis, P. Priswanto, and D. Hermawan, "Design of a Single-phase Radial Flux Permanent Magnet Generator with Variation of the Stator Diameter," *Jurnal Teknologi*, vol. 81, no. 4, June 2019, https://doi.org/10.11113/jt.v81.12889.

[18] J. Faiz, Z. Valipour, M. Shokri-Kojouri, and M. A. Khan, "Design of a Radial Flux Permanent Magnet Wind Generator with Low Coercive Force Magnets," in *2016 2nd International Conference on Intelligent Energy and Power Systems*, Kyiv, Ukraine, June 2016, pp. 1–7, https://doi.org/10.1109/IEPS.2016.7521864.

[19] B. Janarthanan, P. Selvakumar, A. Jagadeeshwaran, and S. Vijayshankar, "Design and Analysis of Multi-phase Permanent Magnet BLDC Generator for Domestic Wind Turbine Applications," in *2014 IEEE 2nd International Conference on Electrical Energy Systems*, Chennai, India, Jan. 2014, pp. 290–293, https://doi.org/10.1109/ICEES.2014.6924183.

[20] P. Xu, K. Shi, Y. Sun, and H. Zhu, "Analytical Model of a Dual Rotor Radial Flux Wind Generator Using Ferrite Magnets," *Energies*, vol. 9, no. 9, Aug. 2016, Art. no. 672, https://doi.org/10.3390/en9090672.

[21] P. J. Randewijk and M. J. Kamper, "Analytical Analysis of a Radial Flux Air-cored Permanent Magnet Machine with a Double-sided Rotor and Non-overlapping Double-layer Windings," in *2012 XXth International Conference on Electrical Machines*, Marseille, France, Sept. 2012, pp. 1178–1184, https://doi.org/10.1109/ICElMach.2012.6350025.

[22] Moh. R. Faqih, S. Sutedjo, and E. Wahjono, "Design and Fabrication of a Radial Flux Permanent Magnet Synchronous Generator," in *2019 International Electronics Symposium*, Surabaya, Indonesia, Sept. 2019, pp. 644–649, https://doi.org/10.1109/ELECSYM.2019.8901620.

[23] E. Flores, M. Cumbajin, and P. Sanchez, "Design of a Synchronous Generator of Permanent Magnets of Radial Flux for a Pico-hydropower Station," in *Advances and Applications in Computer Science, Electronics and Industrial Engineering*, vol. 1307, M. V. García, F. Fernández-peña, and C. Gordón-gallegos, Eds., Singapore: Springer Singapore, 2021, pp. 135–151.

[24] G. G. De Menezes, N. A. R. Maciejewski, E. S. De Carvalho, and T. D. P. M. Bazzo, "A Thorough Procedure to Design Surface-mounted Permanent Magnet Synchronous Generators," *Machines*, vol. 12, no. 6, June 2024, Art. no. 384, https://doi.org/10.3390/machines12060384.

[25] D.-Q. Nguyen, T. N. Thai, C. L. Thi, D. B. Minh, and V. D. Quoc, "Association Between the Analytical Technique and Finite Element Method for Designing SPMSMs with Inner Rotor Type for Electric Vehicle Applications," *Engineering, Technology & Applied Science Research*, vol. 14, no. 3, pp. 14119–14124, June 2024, https://doi.org/10.48084/etasr.7087.

[26] S. A. Dayo, S. H. Memon, M. A. Uqaili, and Z. A. Memon, "LVRT Enhancement of a Grid-tied PMSG-based Wind Farm using Static VAR Compensator," *Engineering, Technology & Applied Science Research*, vol. 11, no. 3, pp. 7146–7151, June 2021, https://doi.org/10.48084/etasr.4147.

[27] T. A. Jumani, Mohd. W. Mustafa, A. S. Alghamdi, M. Md. Rasid, A. Alamgir, and A. B. Awan, "Swarm Intelligence-based Optimization Techniques for Dynamic Response and Power Quality Enhancement of AC Microgrids: A Comprehensive Review," *IEEE Access*, vol. 8, pp. 75986–76001, 2020, https://doi.org/10.1109/ACCESS.2020.2989133.

[28] S. A. Dayo *et al.*, "A New Approach for Improving Dynamic Fault Ride Through Capability of Gridctied Based Wind Turbines," *Scientific Reports*, vol. 15, no. 1, Feb. 2025, Art. no. 6144, https://doi.org/10.1038/s41598-025-89396-0.